Fuel 136 (2014) 89–102

Contents lists available at ScienceDirect

Fuel

journal homepage: www.elsevier.com/locate/fuel

Effects of blending a heavy alcohol ($C_{20}H_{40}O$ with diesel in a heavy-duty compression-ignition engine

A.I. Ramírez [a,*], S.K. Aggarwal [a], S. Som [b], T.P. Rutter [b], D.E. Longman [b]

[a] Department of Mechanical and Industrial Engineering, University of Illinois at Chicago, United States
[b] Center for Transportation Research, Argonne National Laboratory, United States

HIGHLIGHTS

- Feasibility of using phytol ($C_{20}H_{40}O$) with diesel in 5%, 10%, and 20% by volume blends.
- 3-D, transient, turbulent nozzle flow simulations of injection and cavitation of phytol and its blends.
- Single-cylinder engine performance and emissions experiments of the different phytol/diesel blends.
- Combustion event depicted by high-speed natural luminosity imaging using endoscopy.

ARTICLE INFO

Article history:
Received 25 March 2014
Received in revised form 9 June 2014
Accepted 12 June 2014
Available online 6 July 2014

Keywords:
Second-generation biofuel
In-cylinder endoscopy
Bio-derived alcohol
Cavitation modeling
CO and NO_x measurements

ABSTRACT

There is an extensive worldwide search for alternate fuels that can displace fossil-based resources, yet still fit within existing infrastructure. At Argonne National Laboratory, strains of fuel have been designed that are generated by photosynthetic bacteria, eventually producing a heavy alcohol called phytol ($C_{20}H_{40}O$). Phytol's physical and chemical properties (cetane number, heat of combustion, heat of vaporization, density, surface tension, etc.) correspond in magnitude to those of diesel fuel, suggesting that phytol might be a good blending agent in compression ignition (CI) engine applications. The main objective of this study is to investigate the feasibility of using phytol as a blending agent with diesel. Three phytol–diesel blends were chosen for evaluation: P5, P10, and P20 (5%, 10%, and 20% phytol by volume). The fuel blends were extensively analyzed to determine their chemical and physical properties, with mostly comparable values, excepting viscosity and vapor pressure. In order to understand the effects of higher viscosity phytol in the fuel injector, three-dimensional simulations of transient, turbulent nozzle flow compared the injection and cavitation characteristics of the various blends. Specifically, area and discharge coefficients and mass flow rates of diesel and phytol blends were compared under corresponding engine operating conditions. Experimental research was performed using a single-cylinder engine under conventional operating conditions to gather comparative performance and emissions characteristics of the various blends of phytol and diesel. The influence of the fuel's chemical composition on performance and emission characteristics was captured by executing an injection timing sweep. Combustion characteristics such as the in-cylinder pressure trace were comparable for the diesel and all the blends with phytol at each of the injection timings. The diesel/phytol blends show similar emissions characteristics as the diesel. The combustion event was depicted by performing high-speed, natural luminosity endoscopic imaging. The conclusion is that phytol may be a suitable blending agent with diesel fuel for CI applications.

1. Introduction

Second-generation biofuels are an important part of the global plan to develop diverse sources of clean and renewable energy. These alternative fuels can help increase energy security through renewable fuel development while simultaneously reducing emissions from the transportation sector. A major challenge is to identify fuels that are compatible with the current fuel infrastructure, which is geared toward compression-ignition (CI) engines. Using such biofuels as a blending-agent could prolong the use of petrodiesel. An integrated effort to co-develop second-generation biofuels while maintaining engine operation concepts would be timely. Such an approach could expedite the incorporation of second-generation biofuels as blending agents for CI engine applications.

* Corresponding author. Tel.: +1 3124138563.
E-mail address: aramir12@uic.edu (A.I. Ramírez).

http://dx.doi.org/10.1016/j.fuel.2014.06.039
0016-2361/

Nomenclature

C_a	area contraction coefficient
C_d	discharge coefficient
C_v	velocity coefficient
ΔP	difference between injection and back pressure (bar)
ρ_f	fuel density at a specified temperature (kg/m^3)
A_{th}	nozzle exit area (mm^2)
$A_{effective}$	area occupied by the liquid fuel (mm^2)
$\dot{M}_{actual}$	actual (calculated/measured) mass flow rate (g/s)
$\dot{M}_{th}$	theoretical mass flow rate (g/s)

Abbreviations

ATDC	after top dead center
BMEP	brake mean effective pressure
BSFC	brake specific fuel consumption (g/kW h)
BTDC	before top dead center
BTE	brake thermal efficiency (%)
CFD	computational fluid dynamics
CI	compression ignition
ECU	electronic control unit
HCCI	homogeneous charge compression ignition
HEUI	hydraulically actuated, electronically controlled unit injector
HVO	hydrotreated vegetable oil
KH-ACT	Kelvin Helmholtz-aerodynamic cavitation turbulence
PCYLMAX	peak cylinder pressure
PID	proportional-integral-derivative
RNG	renormalization group
ROI	rate of injection
SOI	start of injection
TDR	turbulence dissipation rate
TKE	turbulent kinetic energy

Biodiesels from different feedstocks, such as soy, rapeseed, algae, animal fats, and waste oils, have been extensively investigated as blending agents for CI operation [1–6]. Cuphea-methyl ester [7,8] has also been recently investigated by the U.S. Department of Agriculture as a viable blending agent, since its physical properties are similar to those of diesel. Synthetic fuels, such as hydro-treated vegetable oil (HVO), have received attention in European nations because of their compatibility with the diesel infrastructure and their favorable CI engine characteristics [9,10]. Bio-derived alcohols, such as ethanol and butanol, have been investigated in the past decade as blending agents for diesel fuel. Hansen et al. [11] performed research on ethanol–diesel blends and concluded that further studies are needed to ensure long-term engine durability when these fuel blends are used. Rakopoulos et al. [12,13] blended butanol and diesel at 8% and 16% by volume and analyzed the combustion behavior of a six-cylinder direct injection engine. They found an increase in the ignition delay and reductions in the maximum cylinder pressure and temperature. Iso-pentanol was also recently found to be suitable as a blending agent with gasoline for homogenous charge compression ignition (HCCI) engines [14]. The above literature search reveals that there has been a significant amount of research on incorporating first-generation biofuels in the CI engine infrastructure.

The primary motivation for the present research is to evaluate second-generation biofuels as blending agents for CI engines. Long-chain alcohols, because they have higher energy content than ethanol, butanol, and iso-pentanol, are particularly lucrative alternatives. In metabolic engineering efforts, Argonne National Laboratory (ANL) researchers have designed strains that are produced by photosynthetic bacteria and eventually produce a heavy alcohol called phytol ($C_{20}H_{40}O$), shown in Fig. 1. However, the process is still at a laboratory scale and unable to generate quantities large enough for full-scale engine experiments. The phytol fuel samples for this research were obtained from an outside source [15]. Being an oxygenated fuel, phytol is expected to be environmentally cleaner than petrodiesel (aka "diesel") with respect to particulate matter (PM) emissions [1,16]. Phytol's physical and chemical properties (cetane number, heat of combustion, density, surface tension, etc.) correspond in magnitude to those of diesel fuel (cf. Table 1), suggesting that it might be a good blending agent. Phytol's viscosity, however, is about 20 times higher and vapor pressure is significantly lower than that of diesel fuel, which further encourages studying blends of diesel and phytol, rather than testing pure phytol as a CI engine fuel.

The present study takes a multi-step approach to perform a preliminary assessment of the feasibility of using phytol as a blending agent with diesel fuel under CI engine conditions. Three different blends of phytol (5%, 10%, and 20% by volume) with diesel (i.e. P5, P10, and P20) were studied. The first step involved assessing the physical and chemical properties of the blends. In general, the heat of combustion, density, and cetane number of all five samples were close to each other. Differences in vapor pressure and viscosity were quite significant, however. Note, the vapor pressures of the phytol blends were not measured, but rather were calculated using simple mixing rules. It can be seen that blending the phytol and diesel yielded viscosities closer to that of pure diesel. Since there are significant differences in the viscosities and vapor pressures of neat diesel, neat phytol, and phytol/diesel blends the injection characteristics can be expected to differ. For instance, Som et al. [17] observed that because of differences in vapor pressure, surface tension, and viscosity, the cavitation and turbulence characteristics of soy-based biodiesel and diesel fuels inside the injector were significantly different. The injector flow characteristics determine the boundary conditions at the injector orifice exit, including the rate of injection (ROI) profile as well as the cavitation and turbulence levels; these can have a significant influence on atomization and spray characteristics and consequently on engine performance. Som [18] compared the injection and spray characteristics of diesel and biodiesel (from soy-based feedstock) by using an integrated modeling approach. This approach accounted for the influence in nozzle flow effects, such as cavitation and turbulence [19], on spray-combustion development by using the recently developed Kelvin Helmholtz-Aerodynamic Cavitation Turbulence (KH-ACT) primary breakup model [20]. The simulation identified differences in the spray characteristics of diesel and biodiesel due to variations in nozzle flow characteristics. Specifically, the spray penetration was observed to be higher for biodiesel, while the cone angle was smaller. These results were attributed to the reduced in-nozzle cavitation and turbulence, which resulted

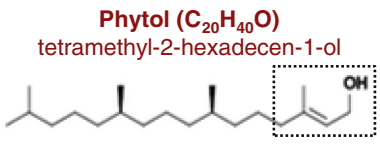

Fig. 1. Chemical structure of phytol.

in slower spray breakup for biodiesel; this, in turn, led to increased fuel penetration.

Thus, the second part of this study was to perform robust in-nozzle flow simulations characterizing the cavitation, turbulence, and flow characteristics of phytol and comparing them to those of diesel fuel. This exercise helps clarify the influence of viscosity and vapor pressure differences on in-nozzle flow development. However, comprehensive computational fluid dynamics (CFD) modeling of phytol/diesel blends for a CI engine simulation are not currently possible. The differences in the physical and chemical properties between phytol and diesel may necessitate the development of new spray, combustion models and chemical kinetic mechanisms before this can be done. Nevertheless the nozzle flow simulations are useful to help characterize the effects of fuel's physical properties, especially due to the challenges associated with the experimental investigation of nozzle flow processes.

The final step of this work is to study the phytol/diesel blends in a single cylinder engine where performance and emissions information is collected. In-cylinder endoscopy was also used to visualize the combustion of the phytol/diesel blends. Since the viscosity differences between pure phytol and diesel were so large, running neat phytol in the engine was not attempted. Further details of this work are in provided in the following sections. Engine and injection system durability tests were not possible because of the small amount of fuel available.

2. Fuel property assessment

Samples of phytol, diesel, and their blends were sent to an external source for analysis of their physical and chemical properties [21,22] where all tests were performed in accordance to ASTM standards [23]. A distillation curve of phytol was produced using gas chromatography. Cetane number was tested by combustion in a constant volume chamber. Heat of combustion was determined in a bomb calorimeter. Note, because of instrumentation limits, it was not possible to accurately measure the vapor pressure of the blends. Hence, it was calculated using simple mixing rules. As indicated in Tables 1 and 2, several of the properties (relative hydrogen content, cetane number, heat of combustion, density, etc.) are not noticeably different for diesel, phytol, and their blends. However, there is significant difference with respect to their viscosity and vapor pressure. Knowledge of these properties is important for both the inner-nozzle computational study, and also for the experimental investigation of the combustion and emission characteristics of the blends.

3. Computational model

The CFD software FLUENT v6.3 was used for 3-D transient turbulent injector flow simulations, which employ a mixture-based approach [24–26]. The two-phase model, called a "full-cavitation model", considered a mixture composed of liquid fuel, vapor, and a non-condensable gas. The gas is compressible, while the liquid is incompressible, but the mixture is considered compressible. A no-slip condition between the liquid and vapor phases was assumed; this assumption was justified due to the fact that the low-pressure cavitating regions were also characterized by the high velocities of the liquid phase; hence, the velocity slip between the phases was rather small [17,29]. The mixture properties were computed by using the Reynolds Averaged continuity and momentum equations [27]. In order to account for large pressure gradients, the Renormalization group $(\mathrm{RNG})_{k-\epsilon}$ turbulence model was incorporated along with the non-equilibrium wall functions. Vapor generation and condensation were calculated by using a linearized form of the Rayleigh–Plesset equation [28]. Then the mixture properties were computed by using the Reynolds-averaged continuity and momentum equations. Further details of the physical model and governing equations can be found in Singhal et al. [29] and Som [18]. The validation of the computational model for in-nozzle flow simulations has been provided in our previous studies [18].

The mini-sac nozzle of the injector studied has six cylindrical holes with a sharp edge at the inlet, and a diameter of 169 μm at an included angle of 126°. The computational domain (single orifice) used in the simulations is indicated by a marked box in Fig. 2. Since the flow was assumed to be symmetric across all the nozzle orifices, only a single orifice was simulated at steady state. Fig. 3 shows the front and back views of the three-dimensional (3-D) sector mesh generated for the same orifice shown in Fig. 2. The sac region was characterized by tetrahedral elements, while other zones consisted of structured orthogonal grids. The pressure values were specified at the inlet and outlet boundaries, while symmetry conditions were employed to demarcate the 60° sector mesh. All the other surfaces were specified as wall boundaries, with no slip between the fuel–fuel/vapor mixture and nozzle orifice walls. A high mesh density was used in the sac region and in the nozzle orifice in order to capture the large pressure and velocity gradients in

Table 1
Comparison of physical and chemical properties of phytol and diesel fuels.

Fuel property	Diesel	Phytol
Carbon content (wt%)	86.64	80.62
Hydrogen content (wt%)	13.01	13.5
Oxygen content (wt%)	0	6.05
Molecular weight (g/mole)	~170	296.54
Sulfur content (ppm)	11.2	<10
Heat of combustion (kJ/kg)	45,500	43,600
Heat of vaporization (kJ/kg)	361	130
Cetane number	47.7	45.9
Density @ 25 °C (kg/m^3)	849.2	850.9
Vapor pressure @ 25 °C (Pa)	1000	<1
Viscosity @ 25 °C (cSt)	3.775	63.54
Boiling point (°C)	320	358

Table 2
Comparison of the physical and chemical properties of phytol, diesel, and three blends.

Fuel property	Diesel	P5	P10	P20	Phytol
Carbon content (wt%)	86.64	86.54	85.87	85.47	80.62
Hydrogen content (wt%)	13.01	13.14	13.11	13.19	13.5
Sulfur content (ppm)	11.2	10.3	10.5	<10	<10
Heat of combustion (kJ/kg)	45,500	45,400	45,400	45,100	43,600
Cetane number	47.7	47.0	46.1	45.9	45.9
Density @ 25 °C (kg/m^3)	849.2	849	849	849.2	850.9
Vapor pressure @ 25 °C (Pa)	1000	950	900	800	<1
Viscosity @ 25 °C (cSt)	3.775	4.115	4.69	6.142	63.54

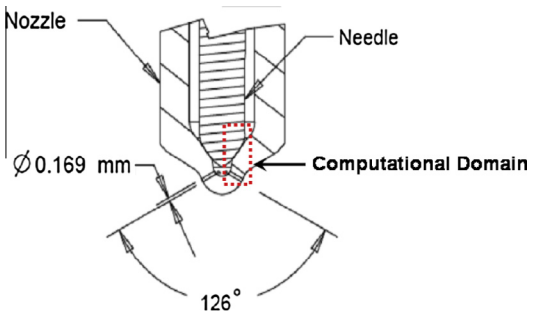

Fig. 2. Schematic of six-hole full-production mini-sac nozzle. Only two holes are seen in this cross-sectional slice. Nozzle and needle regions are identified, along with the computational zone used in simulations. The orifice diameter is 169 μm, with an included angle of 126°.

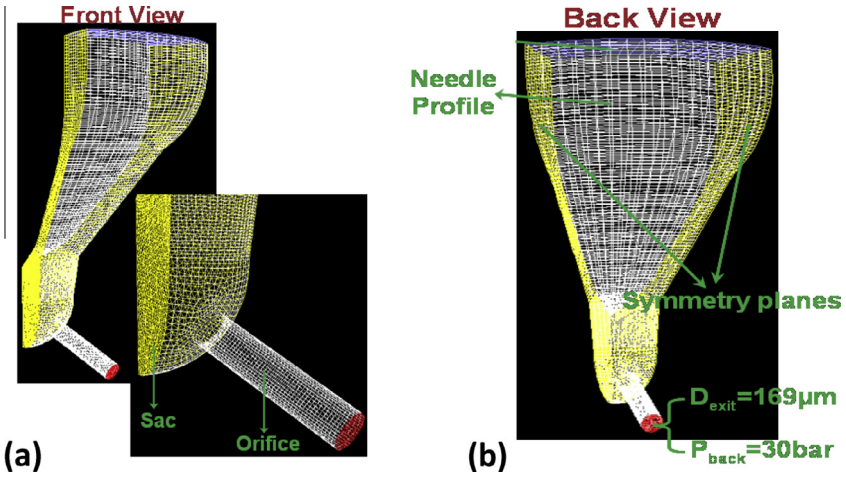

Fig. 3. 3D grid generated for transient nozzle flow simulations.

Table 3
Engine specifications.

Description	Value
Engine model	Caterpillar 3401E
Bore	137.2 mm
Stroke	165.1 mm
Displacement	2.44 L
Compression ratio	16.278:1 (measured on modified cylinder head)
Combustion air system	Simulated turbocharger and air-to-air aftercooler
Fuel injection system	HEUI 315B, six-hole tip

these regions. To obtain grid-convergent solutions, the total number of cells at full-needle-open position was set at close to 120,000. Properties of both liquid and vapor phases were specified.

The measured needle-lift profiles (lift versus time) for this injector were not available, although peak values were known. Wang et al. [30] reported needle lift profiles for a HEUI injection system showing the needle at the full open position for the majority of the injection event. A full needle opening of 275 μm is characteristic of long injection durations and higher load conditions. Simulations were performed with an injection pressure of 1580 bar (cf. Table 4), while the back pressure was fixed at 30 bar. Note that all the fuels mentioned in Table 2 were initialized under the same boundary conditions and with the injection duration of 3 ms.

The discharge coefficient (C_d) and area contraction coefficient (C_a), used to characterize the nozzle flow, are described below. The theoretical mass flow rate can be calculated as:

$$\dot{M}_{th} = A_{th}\sqrt{2 * \rho_f * \Delta P} \tag{1}$$

where ΔP is the difference between injection and back pressure, ρ_f is the fuel density at a specified temperature, and A_{th} is the nozzle exit area. The C_d is calculated from:

$$C_d = \frac{\dot{M}_{actual}}{\dot{M}_{th}} = \frac{\dot{M}_{actual}}{A_{th}\sqrt{2 * \rho_f * \Delta P}} \tag{2}$$

where $\dot{M}_{actual}$ is the mass flow rate calculated from FLUENT simulations. The area contraction coefficient is defined as:

$$C_a = \frac{A_{effective}}{A_{th}} \tag{3}$$

where $A_{effective}$ represents the area occupied by the liquid fuel. C_a is an important parameter for characterizing cavitation, since it is directly influenced by the amount of vapor present at the nozzle exit. The velocity coefficient (C_v) represents the loss in flow velocity due to viscous, turbulent, or cavitation effects. The three coefficients are related as [31]:

$$C_d = C_v * C_a \tag{4}$$

Based on the C_d and C_a, the velocity coefficient (C_v) can be calculated from Eq. (4).

Table 4
Experimental test matrix.

Description	Value
Engine speed	1500 rpm
Intake pressure	1.54 bar
Exhaust pressure	1.39 bar
Injection quantity	100 mm^3/inj
Oil rail pressure	240 bar
(Injection pressure)	(1584 bar)
Fuel	100% diesel
	5% phytol/95% diesel (P5)
	10% phytol/90% diesel (P10)
	20% phytol/80% diesel (P20)
Injection timing	8° BTDC
	4° BTDC
	0° BTDC

4. Experimental setup

A single-cylinder, simulated turbocharged research engine was used to perform these experiments. The injection system employs a Caterpillar hydraulically actuated, electronically controlled unit injector (HEUI) mini-sac with six holes. The HEUI injection system uses hydraulic pressure from the oil to raise the fuel pressure to the desired level for direct injection. This is done by an internal differential piston, which multiplies the relatively modest oil rail pressure to a high fuel injection pressure. This injector uses a pressure intensification ratio of approximately 6.6 between the oil rail pressure and injection pressure [32]. Parameters such as the injection timing, duration, and quantity are controlled by a solenoid that is connected to the engine's Electronic Control Unit (ECU). Details regarding the injector nozzle geometry can be found in Fig. 2, and engine specifications are listed in Table 3. The cylinder head has been modified to provide access ports for endoscope imaging, as discussed later in this section.

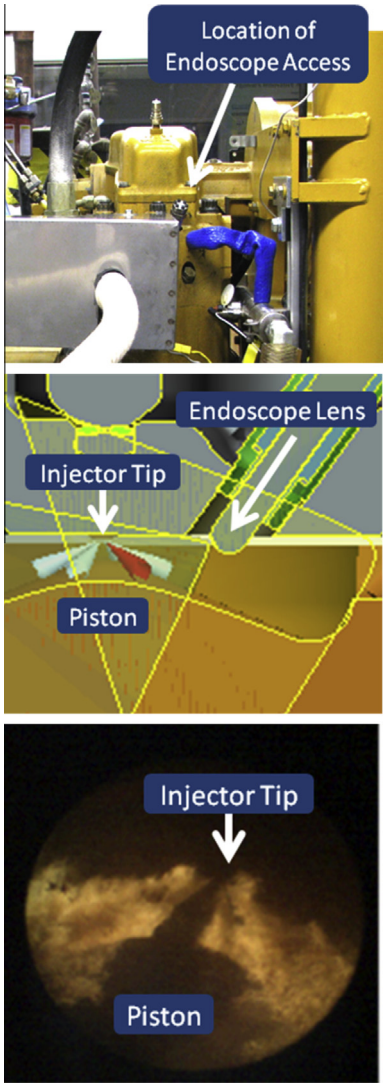

Fig. 4. (top) Single-cylinder engine with marked location of endoscope access in head; (middle) visualization of location of endoscope entry into the combustion chamber; (bottom) sample endoscope image with labeled injector tip and piston crown.

A piezoelectric, water-cooled pressure transducer with a charge amplifier was used to acquire data on the cylinder pressure. The cylinder pressure and crankshaft angle encoder signals were captured using a commercial indicating system and software for data processing [33]. Parameters such as intake/exhaust air pressures and temperatures, engine coolant temperature, engine oil temperature, and others were controlled by using closed-loop proportional-integral-derivative (PID) control through a system that was also used for logging data.

Gaseous emissions were measured by using a chemiluminescent analyzer for volumetric measurements of nitrogen oxides (NO_x), an infrared (IR) analyzer for carbon monoxide (CO) and carbon dioxide (CO_2) measurements, and a paramagnetic detector for O_2 measurements. The fuel flow was modulated and measured by using a fuel balance system that was incorporated into a specially designed fueling cart for low volume experimentation and facilitated switching of fuels. Fuel flow data were logged at a frequency of 1 Hz by the data logging system. More information regarding the test cell setup can be found in previous work [34].

Combustion visualization was performed by using a commercial endoscope system. This system consists of a 4-mm-diameter endoscope and a 640 × 480 pixel, VGA color digital camera with 12-bit resolution. A 60° endoscopic window angle was used to acquire the images presented in this work. Fig. 4 shows the locations of endoscope access and a sample view of the combustion. More details regarding the endoscope system used can be found in other work [35,36].

5. Experimental test matrix

The engine was maintained at a constant speed of 1500 rpm. The engine specifications are provided in Table 3. Since the HEUI injection system is used, the injection pressure is an artifact of oil rail pressure. In this work, the oil rail pressure was kept at 240 bar, which corresponds to a maximum injection pressure of 1584 bar according to the 6.6 ratio of the intensifier piston in the injector [32]. The quantity of fuel injected was maintained at a constant command of 100 mm^3/injection event. There was slight variation in actual delivery, which will be discussed later in the text. Intake and exhaust pressures were maintained at 1.54 and 1.39 bar, respectively. Blends of 5%, 10%, and 20% by volume of phytol (referred to as P5, P10, and P20, respectively) were compared to 100% diesel fuel. An injection timing sweep of three different locations of start of injection (SOI) was performed (8°, 4°, and 0° before top dead center [BTDC]). This results in a total of 12 different conditions, with 9 of them using phytol/diesel blends. Table 4 gives more information on the test matrix. It is important to note how the SOI is controlled in the present set up. The software controlling the injection system allows for an input of SOI location (i.e. 8 deg BTDC). The HEUI uses a double pulse solenoid current to give a single injection event. The internal map in the ECU governs the timing of the actual current executed in engine testing.

6. Results and discussion

6.1. Properties of fuel blends

Distillation curves of phytol and diesel are shown in Fig. 5, where it can be seen that the boiling point for pure phytol is higher than that of diesel. Properties of pure diesel and phytol can be seen in Table 1. Most of the values are similar, with the larger differences in oxygen content, vapor pressure, and viscosity. On a long-term basis, higher viscosity fuel could cause problems such as engine deposits, injector coking, pump failure, and piston ring sticking [37]. The effects of fuel viscosity on engine performance have been widely studied with mixed observations. In regards to combustion, some have seen that higher viscosity could cause a longer physical delay for injection and poorer fuel atomization

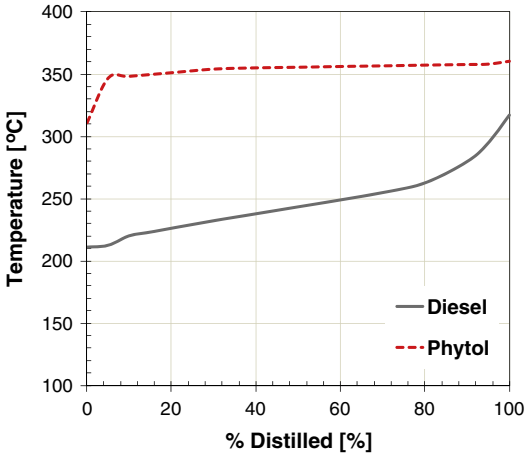

Fig. 5. Distillation curves for diesel and phytol.

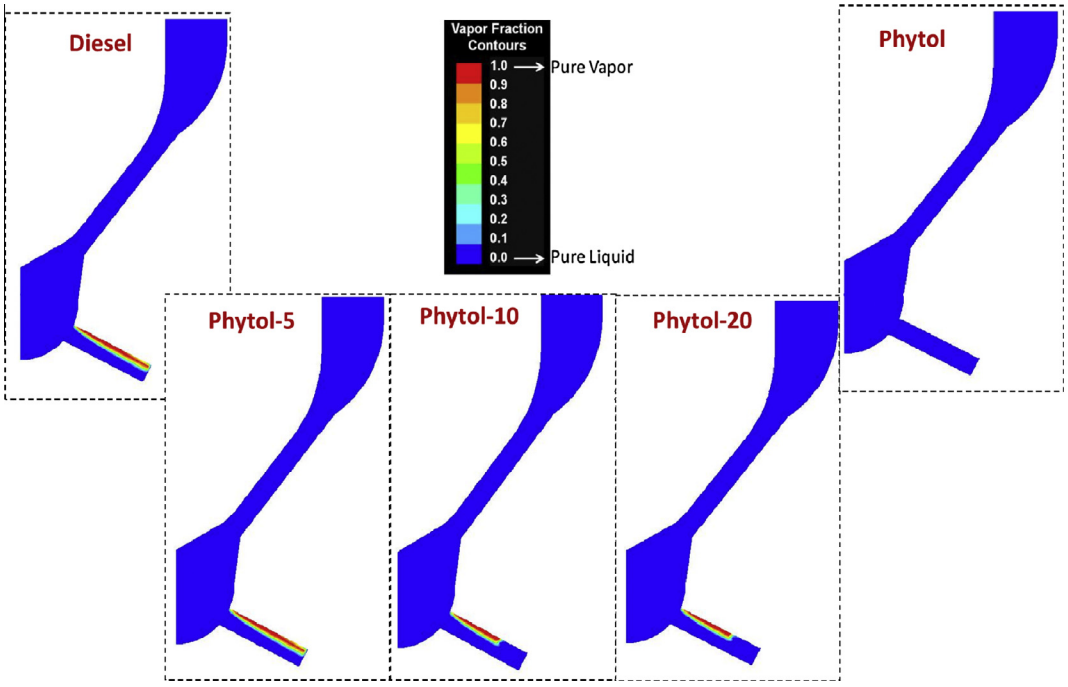

Fig. 6. Vapor fraction contours at the mid-plane for diesel, phytol, and the blends discussed in the context of Table 2.

than the lower viscosity of pure diesel [38]. Others have reported that combined with a higher bulk modulus and sound speed, higher viscosity leads to an advanced start of injection, shifting combustion phasing [39,40]. In the aforementioned studies the injection systems discussed are those with a positive displacement-type pump, thus the advanced SOI with higher viscosity fuel may come from less backflow and losses in the distributor pump. In the present work, a HEUI injector is used, and such effects are not expected. Lower vapor pressure of phytol would lead to less cavitation in comparison to diesel. This was confirmed by our computational results discussed in the next section. Fuels with higher oxygen content should lead to lower soot production in the combustion process [41]. In addition, Graboski et al. [42] performed studies using soybean oil and diesel blends and found good correlation between oxygen content in the fuel and loss of heating value.

Fuel properties of the blends are shown in Table 2. It can be seen that blending brings the blend properties closer to those of pure diesel, and thus more reasonable to run in the engine. Properties listed in Tables 1 and 2 were used in the inner-nozzle simulations.

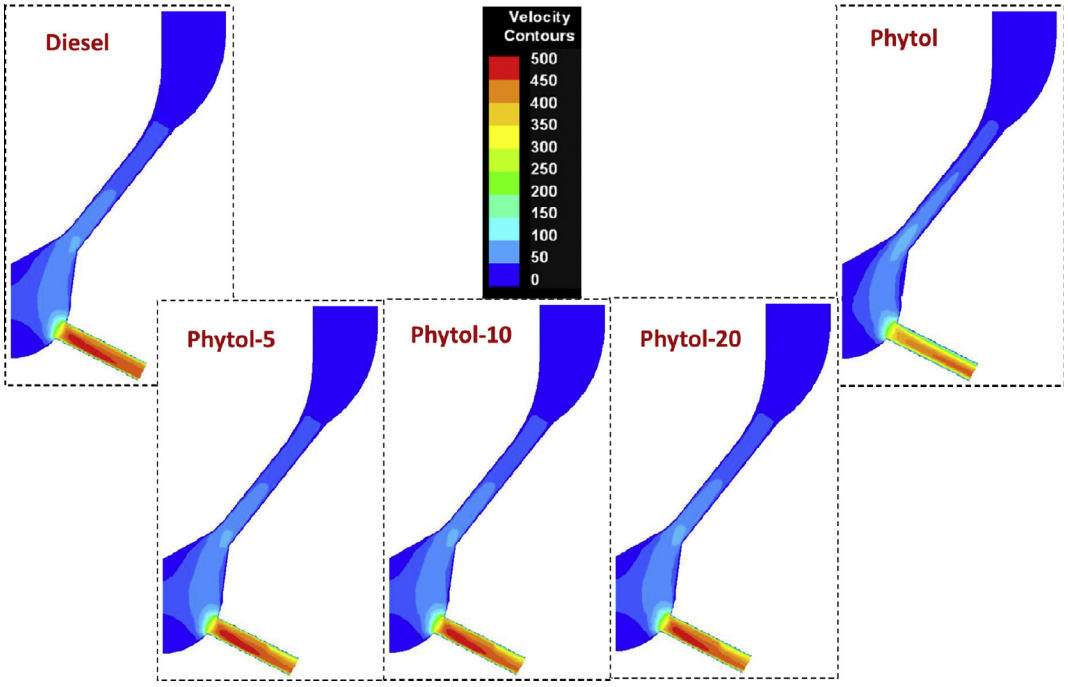

Fig. 7. Velocity contours at the mid-plane for diesel, phytol, and the blends discussed in the context of Table 2.

Table 5
Mass-averaged velocity and turbulence parameters at the nozzle exit, along with quasi-steady values of mass flow rates and discharge and area coefficients for diesel, P5, P10, P20, and phytol.

	Diesel	P5	P10	P20	Phytol
Quasi-steady mass flow rate (g/s)	8.23	8.22	8.29	8.28	6.67
Exit velocity (m/s)	411	410.8	402.7	400	366
Turbulent kinetic energy (m^2/s^2)	2748	2851	3096	3528	2600
Turbulence dissipation rate (m^2/s^3)	5.4E+9	5.5E+9	5.6E+9	6.2E+9	3E+9
t_e (s) (TKE/TDR)	5.1E−7	5.2E−7	5.5E−7	5.7E−7	8.7E−7
Discharge coefficient (C_d)	0.72	0.72	0.73	0.73	0.65
Area coefficient (C_a)	0.90	0.94	1	1	1

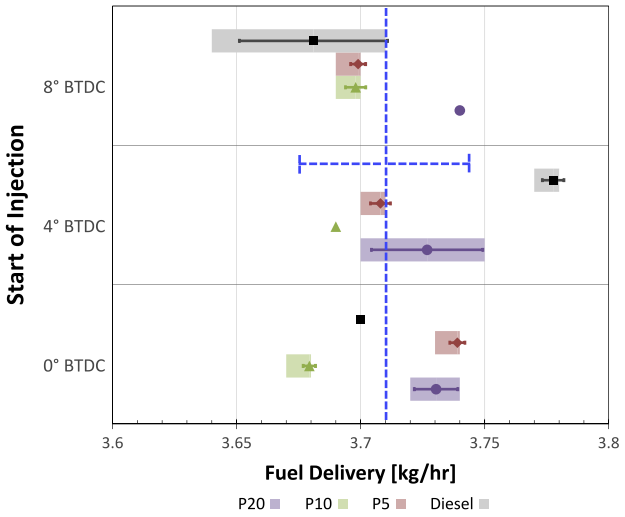

Fig. 8. Actual amount of fuel injected per stroke when maintaining a constant injection quantity command. (Symbols represent the mean, error bars represent plus/minus one standard deviation, and shaded regions show the range of maximum and minimum values. The dashed blue line represents the overall average with plus/minus one standard deviation indicated.) (For interpretation of the references to color in this figure legend, the reader is referred to the web version of this article.)

6.2. Inner-nozzle computational studies

The cavitation model in FLUENT had been validated by the authors in previous studies for high-injection-pressure conditions [18]. Grid variation studies were also performed on the injector in those studies [18]. Hence, additional validations or grid variation studies were not performed.

Fig. 6 plots cavitation contours for all fuels of interest on a 2D mid-plane view at full needle-open position. It should be noted that all nozzle simulations were performed in 3D. No cavitation was observed in the seat region. For diesel fuel, cavitation occurred at the inlet to the orifice, and these patterns reached the orifice exit. Phytol, on the other hand, showed no cavitation.

The viscosity of phytol was higher than that of diesel fuel (cf. Tables 1 and 2). This increased viscosity resulted in lower velocities inside the sac and orifice, which, in turn, decreased the velocity gradients too. This resulted in lowering of cavitation patterns for phytol.

The mid-plane views show that the cavitation characteristics of P5 were similar to those of diesel fuel, with cavitation patterns reaching the orifice exit. This finding was not surprising, since the viscosity was also similar. P10 and P20 showed different cavitation characteristics than those of diesel, phytol, and P5 blend. Although there was a significant amount of cavitation at the orifice inlet, the cavitation patterns were not advected to the nozzle exit.

Fig. 7 plots the velocity contours at the mid-plane for the fuels discussed in the context of Table 2. For all fuels, the velocities inside the orifice and at nozzle exit were quite high because of the elevated injection pressure conditions simulated. The velocities were significantly higher inside the orifice for diesel than for phytol. This was due to the fact that the viscosity of phytol was about 20 times higher than that of diesel fuel. Consequently, velocity magnitude progressively decreases as the amount of phytol in the blend is increased, although the velocity contours for P5, P10, and P20 look fairly similar to that for diesel fuel.

Table 5 shows the mass-averaged exit velocity, turbulent kinetic energy (TKE), and turbulent dissipation rate (TDR) at the nozzle exit. The quasi-steady mass flow rates, discharge and velocity coefficients are also shown for diesel, P5, P10, P20, and phytol. The mass flow rate for phytol was lowest, mainly due to phytol's high viscosity when compared to the viscosities of the other fuels. The mass flow rates at the nozzle exit were similar for the other fuels. P10 and P20 exhibited slightly higher mass flow rates because of the absence of cavitation at the orifice exit. The nozzle exit velocity trends were consistent with the fuel viscosity trends tabulated in Table 2. Diesel fuel had the highest injection velocity, as it had the lowest viscosity. Phytol, on the other hand, had the highest viscosity, resulting in the lowest injection velocities under the conditions investigated. The velocities of P5, P10, and P20 were between those of diesel and phytol. On the basis of averaged TKE and TDR at the nozzle exit, an eddy breakup time scale (t_e) could be estimated [18,19]. Lower values for this time scale generally result in faster turbulent induced breakup. Hence, the turbulence-induced breakup characteristics of diesel and phytol blends can be expected to be generally similar. The turbulence-induced breakup characteristics of phytol are expected to be slowest. The quasi-steady C_d of diesel and phytol blends were found to be similar, whereas the C_d of phytol was the lowest which is consistent with the mass flow rate trends. The quasi-steady C_a values were 1 for P10, P20, and phytol due to absence of cavitation at the nozzle exit. Although cavitation contours of diesel and P5 blends were fairly similar, the C_a was lower for diesel, showing more cavitation at the nozzle exit for diesel. As mentioned earlier, although spray combustion simulations were not performed, the differences in nozzle flow characteristics between diesel and diesel/phytol blend can have an influence on combustion and emission characteristics of the engine. It should be noted that although the differences between pure diesel and phytol fuels for in-nozzle flow development were quite significant, the differences between diesel and diesel/phytol blends were relatively small. Even though these findings cannot be verified experimentally, the CFD simulations provided insights on the injection characteristics of these fuels.

6.3. Experimental investigation

Diesel and phytol/diesel blends were studied in the single-cylinder Caterpillar engine as described previously. Injection pressure (by means of oil rail pressure) and engine speed were held constant. The command for injection quantity was also held constant

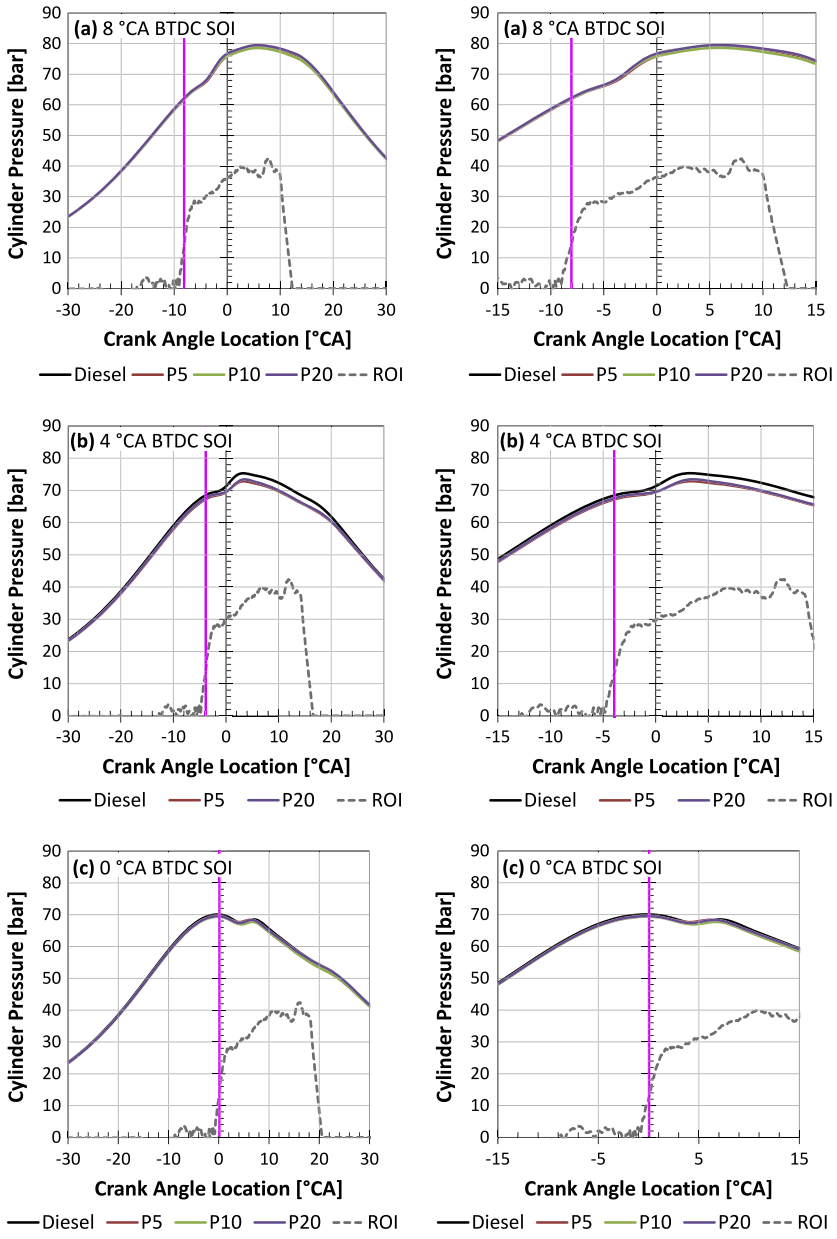

Fig. 9. Cylinder pressure plot of diesel and phytol blends for a case with the injection timing at (a) 8°, (b) 4°, and (c) 0° BTDC. (Zoomed image of each on right, SOI command indicated with pink line.) (For interpretation of the references to color in this figure legend, the reader is referred to the web version of this article.)

Table 6
Peak cylinder pressure values and locations for each of the blends at various start of injection timings. *Note:* for 0° SOI timing case, peak cylinder pressure corresponds to compression pressure and not to combustion pressure.

Start of injection timing (°CA BTDC)	Fuel type	Peak cylinder pressure (bar)		Coefficient of variation (COV)	Location of peak cylinder pressure (°CA BTDC)	
8	Diesel	79.38		0.73	−5.86	
	P5	78.78		0.80	−6.00	
	P10	78.60		0.85	−5.84	
	P20	79.51		0.77	−5.95	
4	Diesel	74.41		0.45	−3.66	
	P5	72.83		0.43	−3.34	
	P10	–		–	–	
	P20	73.43		0.40	−3.53	
0	Diesel	70.05*	68.50†	0.12	−0.19*	−7.00†
	P5	69.57*	68.37†	0.11	0.20*	−6.20†
	P10	69.33*	67.71†	0.20	0.20*	−6.70†
	P20	69.52*	68.32†	0.14	0.22*	−6.60†

* Indicates peak cylinder pressure from compression.
† Indicates peak cylinder pressure from combustion.

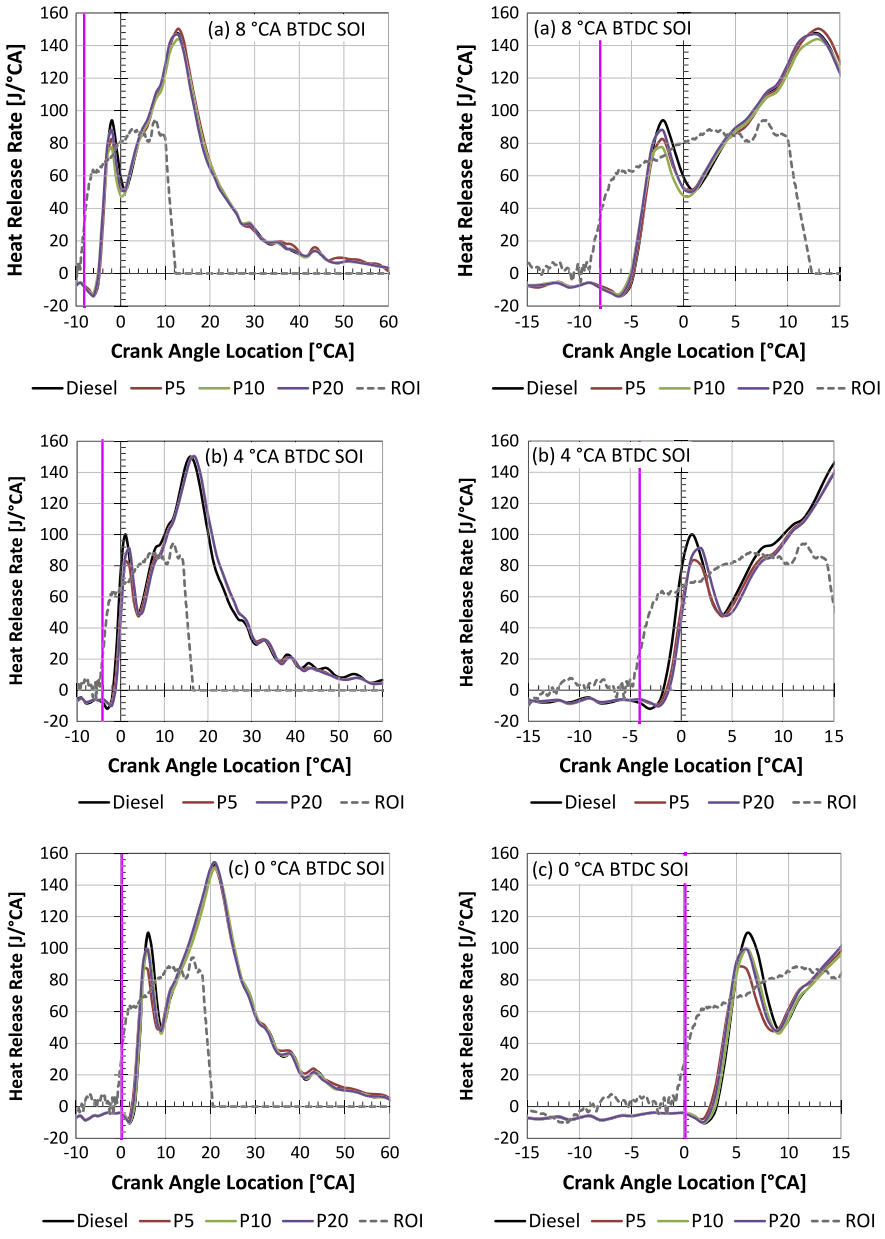

Fig. 10. Heat release rate plot of diesel and phytol blends for a case with the injection timing at (a) 8°, (b) 4°, and (c) 0° BTDC. (Zoomed image of each on right, SOI command indicated with pink line.) (For interpretation of the references to color in this figure legend, the reader is referred to the web version of this article.)

at 100 mm^3/inj; the actual flow amounts are shown in Fig. 8. Tat [39] and Usta [43] have observed higher volume of fuel injected in the case of biodiesel versus diesel and attributed this to the higher viscosity of the biodiesel decreasing backflow in the fuel injection pump. However as mentioned before, the use of a HEUI injection system would not have the same effects. In our study it can be seen by the standard deviation and maximum/minimum flow rates of the different fuel blends, the actual fuel delivery is quite similar across fuel blends. The blending of the biodiesel with the diesel has decreased the disparity in viscosity that is seen with neat fuel.

Fig. 9 compares diesel and the phytol blends in terms of cylinder pressure near the combustion event for the three injection timings of 8°, 4°, and 0° BTDC. For each condition, 100 pressure traces were acquired, and the average pressure trace is shown in the figure. It can be seen that the blended fuels yielded pressure traces similar to those of diesel, with only minor visible differences. Table 6 shows peak pressure values and respective locations in terms of crank angle for each of the SOI cases and various fuel blends. The peak pressure values are close to each other in magnitude, with the largest difference in the 4° SOI case, even then only differing by 1.6 bar. The location of peak pressure is within 0.5 crank angle degrees for all of the cases. The peak pressure decreases as SOI timing retards for all of the fuels tested (cf. Fig. 12). This can be expected as the time available for combustion is decreased as injection gets closer to TDC. This same behavior in which the phytol blends produced results comparable to those of diesel is seen for all injection timings performed.

Fig. 10 plots the heat release rate for the blends of phytol at different SOI timing. Overall there is good similarity between all the cases, although slightly more difference can be seen in the premix burn opposed to the diffusion burn phase of combustion. In the premix burn region the pure diesel shows slightly higher heat release rate than the phytol blends, with the curves collapsing on

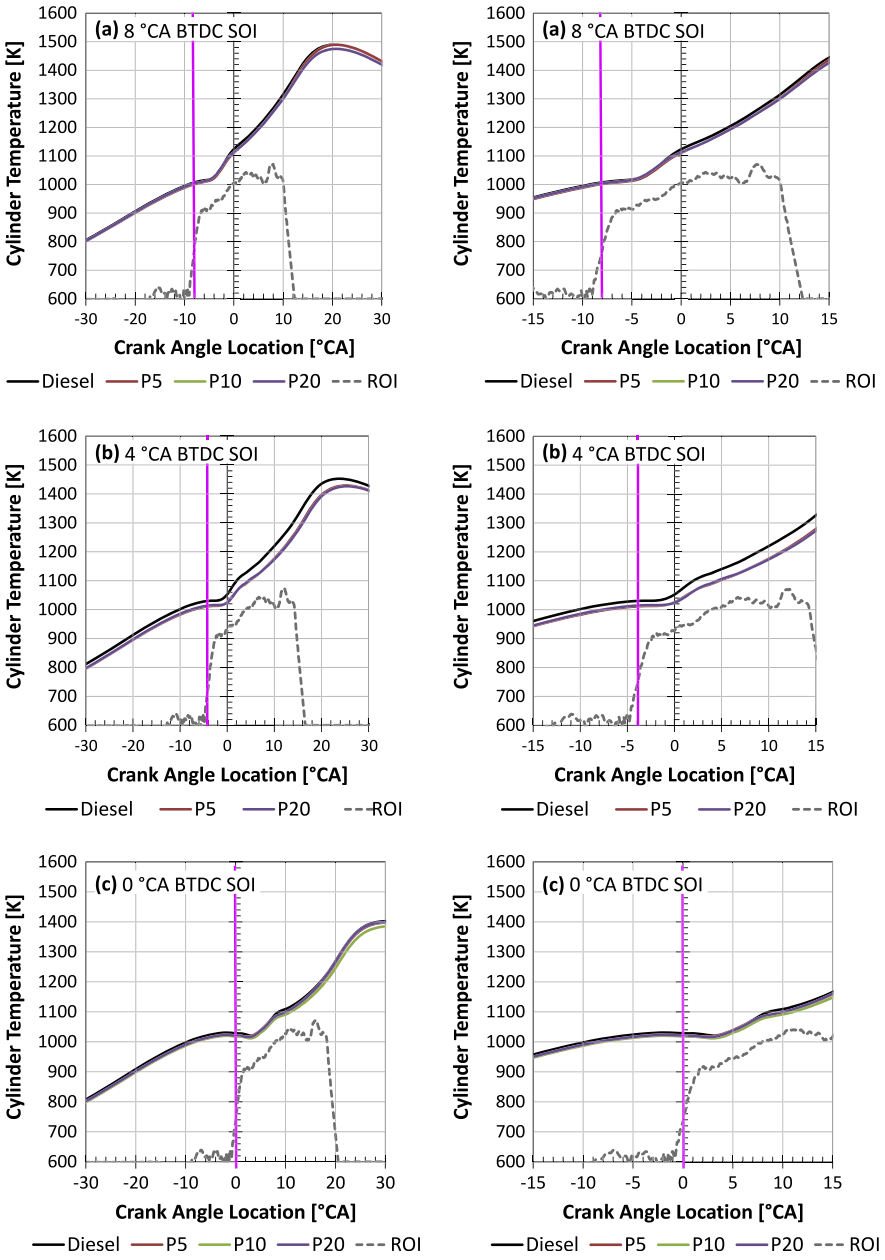

Fig. 11. Cylinder temperature plot of diesel and phytol blends for a case with the injection timing at (a) 8°, (b) 4°, and (c) 0° BTDC. (Zoomed image of each on right, SOI command indicated with pink line.) (For interpretation of the references to color in this figure legend, the reader is referred to the web version of this article.)

each other in the diffusion burn region. This is in agreement with the lower heat of combustion of the phytol/diesel blends versus the pure diesel. These differences are more pronounced as SOI timing approaches TDC. Phasing for the premix and diffusion burns displays good agreement between the blends at all injection timings. Locations of 5%, 10%, 50%, and 90% mass fraction burned are shown in Table 7. It is seen that the blends of phytol yield combustion phasing that is similar to the pure diesel.

Cylinder temperature is shown in Fig. 11 for each of the blends and injection timings. ROI profile is superimposed on the plots in Figs. 9–11 to give an idea of the introduction of the fuel into the cylinder. This rate profile was measured using a Bosch-Type rate meter using a diesel surrogate at the same conditions used in the present work [44]. The solenoid current from engine testing and from these separate rate meter testing are aligned and the corresponding rate profile is shown. Because of the small amount of the fuel available, it was not feasible to obtain rate profiles for the blends. While the rate profiles for the blends may vary slightly from the diesel, they can be used as a conception of injection. Taking a closer look at the SOI command and ROI profile with respect to cylinder temperature it can be seen that the 8, 4, and 0° BTDC SOI timings inject at similar temperatures (~1000–1025 K). However, for the 8° BTDC SOI case the temperature is rising at this point while the temperature for 4° BTDC SOI case the temperature is starting to decline and the 0° BTDC case the temperature has been declining before injection commences. These differences in pressure and temperature in the cylinder will have an effect on combustion, specifically ignition delay. Ignition delay as computed from the difference in SOI command timing to the crank angle location where the heat release rate is 40 J/°CA is reported in Table 8.

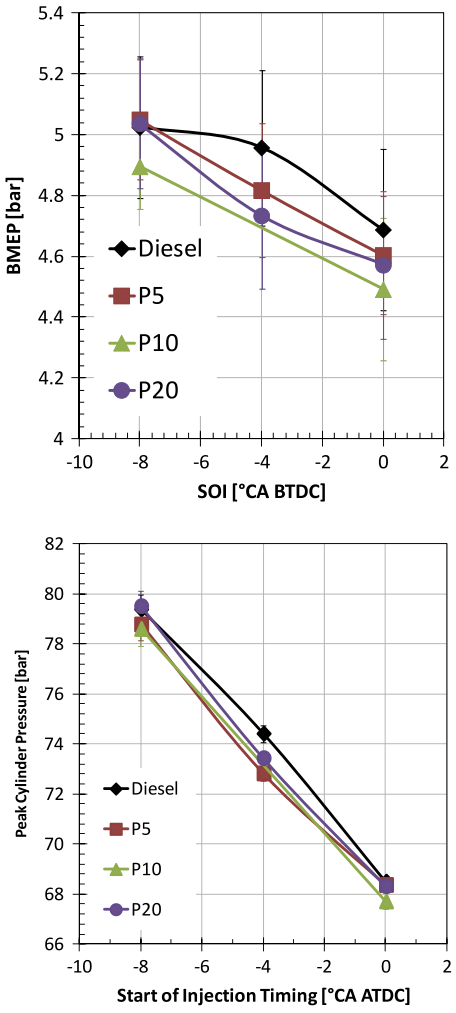

Fig. 12. Peak cylinder pressure and brake mean effective pressure for diesel and phytol blends with respect to start of injection timing.

Table 7
Mass burn fraction (MBF) crank angle locations (shown in °BTDC) for each of the blends at the various start of injection timings.

	Diesel	P5	P10	P20
8° CA BTDC SOI				
5% MBF	0.30	0.22	0.05	0.40
10% MBF	−2.05	−2.33	−2.50	−2.10
50% MBF	−13.00	−13.12	−13.25	−12.90
90% MBF	−30.35	−31.27	−30.75	−30.65
4° CA BTDC SOI				
5% MBF	−3.91	−4.20	–	−4.05
10% MBF	−6.34	−6.60	–	−6.48
50% MBF	−17.15	−17.25	–	−17.23
90% MBF	−34.39	−34.80	–	−34.23
0° CA BTDC SOI				
5% MBF	−7.85	−7.85	−7.95	−7.78
10% MBF	−10.20	−10.50	−10.50	−10.35
50% MBF	−21.50	−21.60	−21.80	−21.43
90% MBF	−38.60	−39.35	−38.90	−38.58

Lapuerta et al. describe a variety of studies with biodiesel from different feedstocks [45]. A reduced BMEP is seen in some cases corresponding to the decreased lower heating value of the biodiesel used versus diesel. However, some groups have observed very small loss or even an increase in power using biodiesel [43,46,47]. This power recovery was explained by the increased

Table 8
Ignition delay (shown in °CA) as computed from SOI command to time taken to reach a heat release rate of 40 J/°CA for each of the SOI timings and fuel blends.

	Diesel	P5	P10	P20
8° CA BTDC SOI	4.23	4.22	4.05	4.04
4° CA BTDC SOI	3.27	3.70	–	3.85
0° CA BTDC SOI	4.13	3.67	4.03	3.78

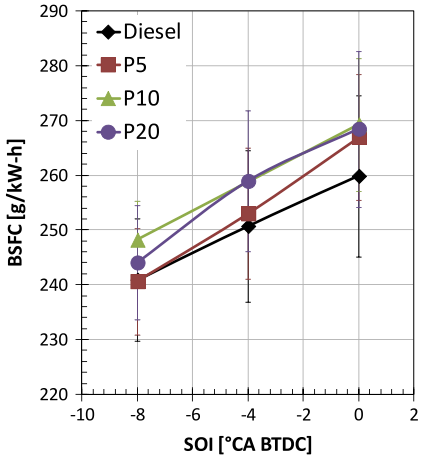

Fig. 13. Brake specific fuel consumption of diesel and the phytol/diesel blends at various SOI timings.

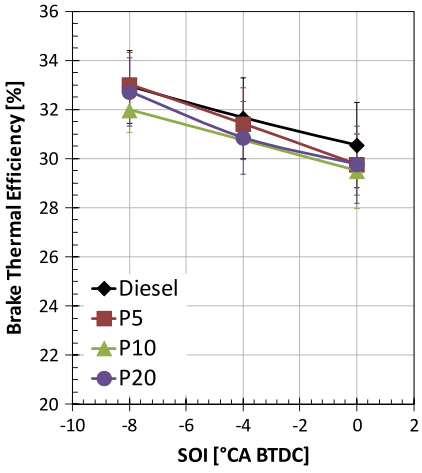

Fig. 14. Brake thermal efficiency of diesel and the phytol/diesel blends at various SOI timings.

density and viscosity which could lead to advanced start of injection and fewer injection pump losses, in addition to improved combustion of the biodiesel since it is an oxygenated fuel. A shift of the combustion phasing would also result from advanced SOI timing. Fig. 12 shows variations in peak cylinder pressure (PCYLMAX) and brake mean effective pressure (BMEP) with respect to the SOI timing using the diesel and phytol blends from the present work. Bars representing one standard deviation are shown on the plot, indicating repeatability. For both BMEP and peak pressure, diesel is slightly higher than the phytol/diesel blends. Although all of the values are close, the greatest variability is seen at an SOI timing of 4 deg before TDC (4% and 2% difference between the maximum and minimum values in BMEP and peak pressure respectively). It may be anticipated that phytol/diesel blends would yield a lower power as a result of the lower heat of combustion of the fuel. Also, the reduced cetane number of the blends

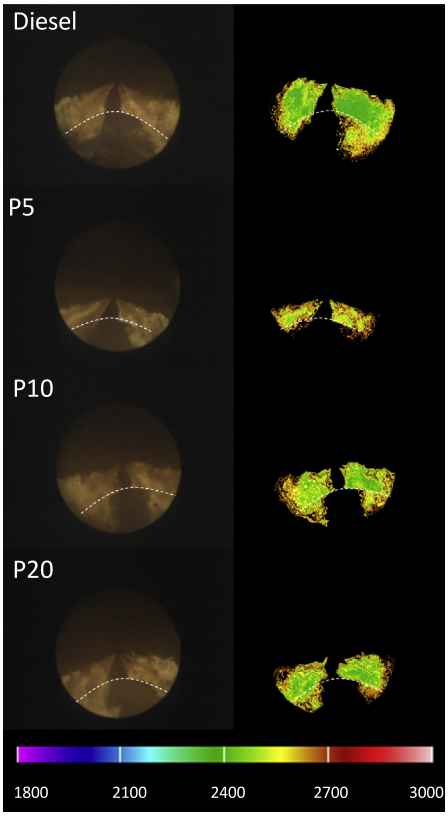

Fig. 15. (left) Combustion imaging and (right) temperature distribution of the 8° BTDC injection timing case for diesel and phytol blends shown at 4° ATDC; piston crown is indicated by dashed white line.

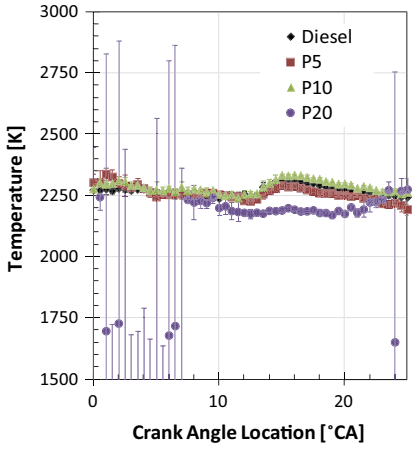

Fig. 16. Average soot radiation temperature for diesel and phytol blends for the 8° BTDC SOI condition.

suggests a lower attainable peak pressure. Although we do not have information on differences of SOI of the blends with respect to the pure diesel, no significant differences in combustion phasing are apparent (cf. Fig. 10 and Table 7). As is suggested by the inner-nozzle simulations performed, cavitation is lower for the blended fuels (primarily P10 and P20) due to the difference in viscosity. This reduced cavitation and higher viscosity may lead to poorer atomization of the fuel. These effects combined with the lower cetane number for the blends may be responsible for the lower BMEP and peak pressures compared to pure diesel fuel. This is more apparent at later SOI timing, i.e., 4° and 0° BTDC. It seems that combustion is not fully developed resulting in marginally lower

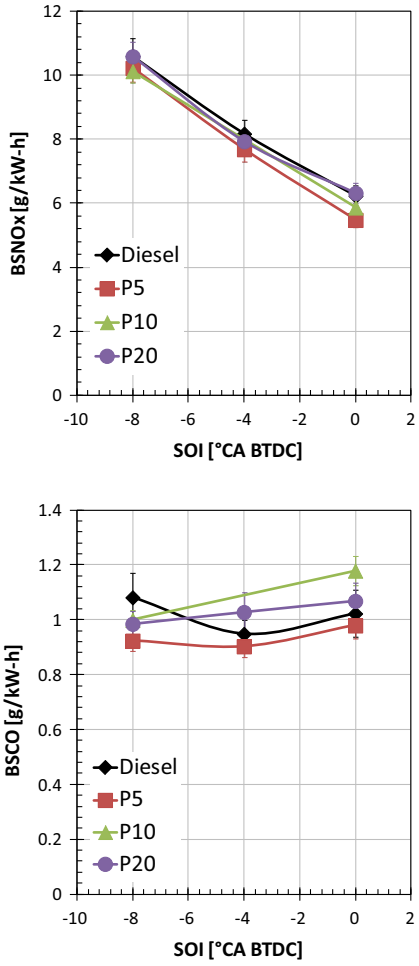

Fig. 17. NO_x and CO as a function of injection timing.

peak pressure and less power for the blends. Still, the values yielded for BMEP and peak pressure are quite close to each other, reflective of a interplay between the various properties of pure diesel and the blends that are expected to lower power output (lower heat of combustion, lower vapor pressure, higher viscosity, and lower cetane number) and those that could contribute to power recovery (higher oxygen content).

Brake Specific Fuel Consumption (BSFC), the ratio of fuel flow rate to power, is shown in Fig. 13 for all the phytol/diesel blends and injection timings. It can be seen that BSFC is higher for the phytol/diesel blends than it is for pure diesel at the varied SOI timings. Fuel flow rates for all of the fuels used were comparable (cf. Fig. 8), while power generated was lower for the blends. This can be attributed to the lower heat of combustion of the phytol blends versus that of diesel. Phytol has a higher oxygen content, which is an indicator of loss of heating value of the fuel, and thus an expected increase in fuel consumption. Rakopoulos et al. showed that there was increase in BSFC only when the oxygen increase is from the fuel and not from the intake air [48]. It is not the volume of the fuel, rather its energy that yields power. Thus, the reduction in heat of combustion in the blends can contribute to the lower power and therefore the higher BSFC is observed with the blends.

Brake Thermal Efficiency (BTE) may be a more suitable measure for performance of the fuels since it takes into account the differences in heat of combustion of the fuel. This quantity represents the ratio of the engine's power output to the energy input (product of fuel mass flow rate and lower heating value). BTE for the diesel and phytol/diesel blends at each SOI timing is shown in Fig. 14. BTE values are close to each other for diesel and blends at all SOI

timings, with diesel showing higher efficiency than the blends. Largest differences are seen at an SOI timing of 0 deg before TDC with a 3.4% loss of efficiency using blends versus diesel. Since BTE takes into account the difference in heating value of the fuel, it seems that lower cetane number and vapor pressure are showing effect here by having a lower power output at similar fuel delivery.

Combustion imaging was performed for each of the blends for all injection timing conditions. Fig. 15 shows sample images for the 8° SOI case at a location 4° after top dead center (ATDC). The endoscope must be removed when switching fuel sources in order to clean the window. Its removal and reinsertion can lead to variability in the image perspective, which can be seen in the figure. The endoscope enters the combustion chamber just between two of the six plumes on the nozzle tip. In each of the images, the top of the piston crown is indicated by the dashed line. With the injector nozzle located at the center of the image, two spray plumes are clearly visible in the front of the image. Adjacent sprays can be seen in the background too. An inspection of the combustion images (left side of Fig. 15) reveals no discernible differences. The images can be used to perform two-color optical pyrometry to calculate the soot radiation temperature, as described in other studies. [33,49–51]. The right side of Fig. 15 shows the temperature distributions as calculated from the combustion images on the left. Qualitatively it can be seen in all cases that the higher temperatures are found around the periphery of the spray. This finding is consistent with the conceptual combustion model described by Dec [52]. At this point, it is difficult to make any generalizations about the in-cylinder combustion from the images obtained. Improvements to the camera repositioning after cleaning are needed to better quantify the combustion image variations observed. This is illustrated specifically in the P5 case where it appears that the combustion cloud is actually smaller, when in actuality the image perspective is altered by camera positioning.

Each condition was tested twice with 4 repetitions each, resulting in 8 distinct measurements taken for each data point. Quantitative temperature results are shown in Fig. 16 for the SOI timing of 8° BTDC. The data represented here shows the average of these 8 points with error bars representing the standard deviation at each location. This plot verifies that the average temperatures of diesel and the blends are close, although the values are slightly higher for diesel. This was consistent with the marginally higher thermal NO_x emissions obtained with diesel, as indicated in Fig. 17a.

There is a high level of scatter seen for the P20 case towards the start of the cycle. This may be indicative of some instability caused by some differences in the fuel properties for this blend. Note that the temperature becomes much more stable towards 8 deg after TDC. At this point, the injection event has ended, and there is no longer fuel entering the cylinder. Further studies on repeatability during the time of injection would be valuable to understand this behavior.

With regards to NO_x emissions with biodiesel and its blends with diesel, typically NO_x emissions increase with the percentage of biodiesel in the blend [53]. This has been explained by the advanced combustion phasing resulting from the physical properties of biodiesel that might yield an earlier SOI, which would produce higher temperatures in the engine cylinder. Other researchers have seen a decrease in NO_x emissions when using biodiesel [54,55]. However, as discussed previously, SOI variation due to different fuels are not expected with the HEUI injection system. In the present work, lower temperature is observed for the diesel/phytol blends, which supports the lower NO_x emissions compared to diesel, as shown in Fig. 17a. This lower temperature is a result to differences in mixing and combustion with the blends.

Generally, it is perceived that the increased oxygen content in biofuel would lead to more complete combustion and thus reduce CO emissions [45,56]. Ullman et al. showed that as cetane number and fuel oxygen content increase, CO emissions decrease [57]. In the present study, as the amount of phytol in the blend increases, oxygen content increases while cetane number decreases. Fig. 17b plots CO versus SOI timing for diesel and phytol blends. At advanced SOI command timing (8 deg before TDC), diesel has higher CO emissions. This trend shifts as injection timing is brought closer to TDC, with respect to CO emissions from pure diesel. Higher CO emissions from the P20 blend is seen at 4° BTDC, and from both P20 and P10 blends at 0° BTDC. It appears in the present study that there is an interplay between the oxygen content and the cetane number of the blends which is affected by combustion phasing (as a result of injection timing) as is seen in Fig. 17b.

7. Conclusions

This work performs a study of a biologically-derived heavy alcohol called phytol ($C_{20}H_{40}O$) and its potential for displacement of petrodiesel. First a property analysis of diesel, pure phytol, and 5%, 10%, and 20% phytol/diesel blends was performed. The assessment of phytol's physical and chemical properties revealed that it may be a suitable agent for blending with diesel fuel for CI engine applications. CFD modeling was performed to study the effects of the phytol on the inner-nozzle behavior of the fuels. With this knowledge, an experimental study was conducted to analyze the performance and emissions of these blends in a single-cylinder compression ignition engine. Important observations are as follows:

(1) According to nozzle flow simulations, the physical properties of phytol affect the spray atomization characteristics at blends higher than 5% phytol/95% diesel.
(2) According to experimental work, differences noticed in performance and emissions between diesel and phytol/diesel blends are small – indicating that phytol may be suitable as a blending agent with diesel. Simulations suggested that neat phytol fuel is not suitable for engine studies; thus, engine testing with this fuel was not attempted.
(3) No significant differences in combustion phasing are visible in the range of blends used. This suggests that either there is not much difference in SOI, or the effects of the phytol/diesel properties counteract any of the effects of altered SOI timing.
(4) NO_x and CO emissions resulting from the phytol/diesel blends are similar to those exhibited by the pure diesel. NO_x emissions of the blends are nearly identical with slightly lower values for the phytol/diesel blends. A consistent trend in CO emissions is not apparent.
(5) In the case of advanced injection timing (8 deg BTDC) there is greater tolerance for differences in the fuel, while the retarded injection timing case (0 deg BTDC) shows slight differences.
(6) There is instability towards the start of the combustion event that is apparent in the P20 blend. This scatter stabilizes once the injection event is over. Further studies on repeatability during the injection event for this blend would be valuable in the future.

On the basis of the findings of this scoping study, future research will focus on a comprehensive assessment of engine durability. Because of the differences in oxygen content of the fuel, it would also be beneficial to perform studies on particulate emissions. Rate of injection (ROI) studies would be useful to understand some impact of the physical properties of phytol on the spray and combustion. Complementary studies are also being done to assess the life-cycle of phytol to understand the energy balance involved

in engineering phytol and the potential scope of implementing phytol in a large-scale infrastructure. Comprehensive CFD modeling can expedite the large-scale incorporation of phytol for CI engines and optimize the performance of this fuel. All of these studies would require more phytol than was available at the time of the present study.

Acknowledgments

The submitted manuscript has been created by UChicago Argonne, LLC, operator of Argonne National Laboratory (Argonne). Argonne, a U.S. Department of Energy Office of Science laboratory, is operated under Contract No. DE-AC02-06CH11357. The U.S. Government retains for itself, and others acting on its behalf, a paid-up, nonexclusive, irrevocable worldwide license in said article to reproduce, prepare derivative works, distribute copies to the public, and perform publicly and display publicly, by or on behalf of the Government.

This research was funded by DOE's Office of Vehicle Technologies, Office of Energy Efficiency and Renewable Energy under Contract No. DE-AC02-06CH11357. The authors wish to thank Kevin Stork, program manager at DOE, for his support.

References

[1] Graboski MS, McCormick RL. Combustion of fat and vegetable oil derived fuels in diesel engines. Prog Energy Combust Sci 1998;24:125–64.
[2] Armas O, Hernandez J, Cardenas M. Reduction of diesel smoke opacity from vegetable oil methyl esters during transient operation. Fuel 2006;85:2427–38.
[3] Grimaldi CN, Postrioti L, Battistoni M, Millo F. Common rail HSDI diesel engine combustion and emissions with fossil/bio-derived fuel blends. SAE Paper No. 2002-01-0865; 2002.
[4] Hashimoto M, Dan T, Asano I, Arakawa T, Combustion of the rape-seed oil in a diesel engine. SAE Paper No. 2002-01-0865; 2002.
[5] Agarwal AK. Performance evaluation and tribological studies on a biodiesel fuelled compression ignition engine. PhD thesis. Indian Institute of Technology, Delhi; 1999.
[6] Higgins BS, Mueller CJ, Siebers DL. Measurements of fuel effects on liquid-phase penetration in DI sprays. SAE Paper No. 1999-01-0519; 1999.
[7] Knothe G, Cermak SC, Evangelista RL. Cuphea oil as source of biodiesel with improved fuel properties caused by high content of methyl decanoate. Energy Fuels 2009;23:1743–7.
[8] Fisher BT, Knothe G, Mueller CJ. Liquid phase penetration under unsteady in-cylinder conditions: soy- and cuphea-dervied biodiesel fuels versus conventional diesel. Energy Fuel 2010;24:5163–80.
[9] Aatola H, Larmi M, Sarjovaara T, Mikkonen S. Hydrotreated vegetable oil (HVO) as a renewable diesel fuel: trade-off between NOx, particulate emission, and fuel consumption of a heavy duty engine. SAE Paper No. 2008-01-2500; 2008.
[10] Gong Y, Kaario O, Tilli A, Larmi M, Tanner FX. A computational investigation of hydrotreated vegetable oil sprays using RANS and a modified version of the RNG k–ε model in OpenFOAM. SAE Paper No. 2010-01-0739; 2010.
[11] Hansen AC, Zhang Q, Lyne PWL. Ethanol-diesel fuel blends – a review. Bioresour Technol 2005;96:277–85.
[12] Rakopoulos DC, Rakopoulos CD, Papagiannakis RG, Kyritsis DC. Combustion heat release analysis of ethanol or n-butanol diesel fuel blends in heavy-duty DI diesel engine. Fuel 2011;90:1855–67.
[13] Rakopoulos DC, Rakopoulos CD, Hountalas DT, Kararas EC, Giakoumis EG, Papagiannakis RG. Investigation of the performance and emissions of bus engine operating on butanol/diesel fuel blends. Fuel 2010;89:2781–90.
[14] Yang Y, Dec J, Dronniou N, Simmons B. Characteristics of isopentanol as a fuel for HCCI engines. SAE Paper No. 2010-01-2164.
[15] www.sigmaaldrich.com/united-states.html.
[16] Lapuerta M, Armas O, Ballesteros R. Diesel particulate emissions from biofuels derived from Spanish vegetable oils. SAE Paper No. 2002-01-1657; 2002.
[17] Som S, Longman DE, Ramírez AI, Aggarwal SK. A comparison of injector flow and spray characteristics of biodiesel with petrodiesel. Fuel 2010;89:4014–24.
[18] Som S. Development and validation of spray models for investigating diesel engine combustion and emissions. PhD thesis. University of Illinois at Chicago; 2009.
[19] Som S, Ramírez AI, Longman DE, Aggarwal SK. Effect of nozzle orifice geometry on spray, combustion, and emission characteristics under diesel engine conditions. Fuel 2011;90:1267–76.
[20] Som S, Aggarwal SK. Effects of primary breakup modeling on spray and combustion characteristics of compression ignition engines. Combust Flame 2010;157:1179–93.
[21] http://www.swri.org/4org/d08/petprod/fuelana/home.htm.
[22] http://www.astm.org/LABS/filtrexx40.cgi?+-P+ACCTNO+82650+template.frm.
[23] http://www.astm.org/.
[24] FLUENT v6.3 documentation; 2006.
[25] Li H, Kelecy F, Egelja-Maruszewski A, Vasquez SA. Advanced computational modeling of steady and unsteady cavitating flows. IMECE 2008:2008–67450.
[26] Payri R, Margot X, Salvador FJ. A numerical study of the influence of diesel nozzle geometry on the inner cavitating flow. SAE Paper No. 2002-01-0215; 2002.
[27] Jia M, Hou D, Li J, Xie M, Liu H. A micro-variable circular orifice fuel injector for HCCI-conventional engine combustion – Part 1, Numerical simulation of cavitation. SAE Paper No. 2007-01-0249; 2007.
[28] Brennen EC. Cavitation and bubble dynamics. Oxford University Press; 1995.
[29] Singhal AK, Athavale AK, Li H, Jiang Y. Mathematical basis and validation of the full cavitation model. J Fluid Eng 2002;124:617–24.
[30] Wang T-C, Han J-S, Xie X-B, Lai M-C, Henein NA, Schwarz E, et al. Parametric characterization of high-pressure diesel fuel injection systems. Trans ASME 2003;125:412–26.
[31] Siebers DL. Liquid-phase fuel penetration in diesel sprays. SAE Paper No. 980809; 1998.
[32] Yudanov SV. Development of the hydraulically actuated electronically controlled unit injector for diesel engines. SAE 952057; 1995.
[33] https://www.avl.com/its.
[34] Longman DE. In-cylinder injection of oxygen enriched air to reduce diesel engine exhaust emissions. Master of Science Thesis. University of Illinois at Chicago; 2006.
[35] AVL ThermoVisionTM Manual, March; 2004.
[36] Ciatti SA, Miers SA, Ng HK. Influence of EGR on soot/NOx production in a light-duty diesel engine. ASME-ICEF 2005-1327; 2005.
[37] Kegl B. Effects of biodiesel on emissions of a bus diesel engine. Bioresour Technol 2000;99(4):863–73.
[38] Machacon HTC, Shiga S, Karasawa T, Nakamura H. Performance and emission characteristics of a diesel engine fueled with coconut oil–diesel fuel blend. Biomass Bioenergy 2000;20:63–9.
[39] Tat ME. Investigation of oxides of nitrogen emissions from biodiesel-fueled engines. Ph.D. thesis. Iowa State University; 2003.
[40] Monyem A, Van Gerpen JH, Canakci M. The effect of timing and oxidation on emissions from biodoesel-fueled engines. Trans ASAE 2001;44(1):35–42.
[41] Schmidt K, Van Gerpen JH. The effect of biodiesel fuel composition on diesel combustion and emissions. SAE Paper No. 961086; 1996.
[42] Graboski MS, Ross JD, McCormick RL. Transient emissions from no. 2 Diesel and Biodiesel Blends in a DDC Series 60 Engine. SAE 961166; 1996.
[43] Usta N. An experimental study on performance and exhaust emissions of a diesel engine fuelled with tobacco seed oil methyl ester. Energy Convers Manage 2005;46:2373–86.
[44] Bosch W. The fuel rate indicator: a new measuring instrument for display of the characteristics of individual injection. SAE 660749; 1966.
[45] Lapuerta M, Armas O, Rodriguez-Fernandez J. Effect of biodiesel fuels on diesel engine emissions. Prog Energy Combust Sci 2008;34:198–223.
[46] Carrareto C, Macor A, Mirandola A, Stoppato A, Tonon S. Biodiesel as alternative fuel: experimental analysis and energetic evaluations. Energy 2004;29:241–6.
[47] Silva FN, Prata AS, Teixeira JR. Technical feasibility assessment of oleic sunflower methyl ester utilization in diesel bus engines. Energy Convers Manage 2003;44:2857–78.
[48] Rakopoulos CD, Hountalas DT, Zannis TC, Levendis YA. Operational and environmental evaluation of diesel engines burning oxygen-enriched fuels: a review. SAE 2004-01-2924; 2004.
[49] Zhao H, Ladommatos N. Optical diagnostics for soot and temperature measurement in diesel engines. Prog Energy Combust Sci 1998;4(3):221–56.
[50] Shiozaki T, Nakajima H, Yojota H, Miyashita A. The visualization and its analysis of combustión flame in DI Diesel Engine. SAE 980141; 1998.
[51] Ciatti SA, Blobaum EL, Foster DE. Determination of diesel injector nozzle characteristics using two-color optical pyrometry. SAE 2002-01-0746; 2002.
[52] Dec JE. A conceptual model of DI diesel combustion based on laser-sheet imaging. SAE Paper No. 970873; 1997.
[53] Assessment and Standards Division (Office of Transportation and Air Quality of the US Environmental Protection Agency). A Comprehensive Analysis of Biodiesel Impacts on Exhaust Emissions. EPA 420-P02-001; 2002.
[54] Peterson CL, Reece DL. Emissions testing with blends of esters of rapeseed oil fuel with and without a catalytic converter. SAE Paper 961114; 1996.
[55] Lapuerta M, Armas O, Ballesteros R, Fernandez J. Diesel emissions from biofuels derived from Spanish potential vegetable oils. Fuel 2005;84:773–80.
[56] Agarwal A. Biofuels (alcohols and biodiesel) applications as fuels for internal combustion engines. Prog Energy Combust Sci 2007;33:233–71.
[57] Ullman TL, Spreen KB, Mason RL. Effects of cetane number, cetane improver, aromatics, and oxygenates on 1994 heavy-duty diesel engine emissions. SAE Paper 941020; 1994.